remote sensing

Article

Spatial Variability of Raindrop Size Distribution at Beijing City Scale and Its Implications for Polarimetric Radar QPE

Zhe Zhang [1], Huiqi Li [2], Donghuan Li [3] and Youcun Qi [3,*]

1 Shenzhen National Climate Observatory, Shenzhen 518040, China
2 Guangzhou Institute of Tropical and Marine Meteorology, China Meteorological Administration/China Meteorological Administration Tornado Key Laboratory, Guangzhou 510640, China
3 Key Laboratory of Water Cycle and Related Land Surface Processes, Institute of Geographic Sciences and Natural Resources Research, Chinese Academy of Sciences, Beijing 100101, China
* Correspondence: youcun.qi@igsnrr.ac.cn

Abstract: Understanding the characteristics of the raindrop size distribution (DSD) is crucial to improve our knowledge of the microphysical processes of precipitation and to improve the accuracy of radar quantitative precipitation estimation (QPE). In this study, the spatial variability of DSD in different regions of Beijing and its influence on radar QPE are analyzed using 11 disdrometers. The DSD data are categorized into three regions: Urban, suburban, and mountainous according to their locations. The DSD exhibits evidently different characteristics in the urban, suburban, and mountain regions of Beijing. The average raindrop diameter is smaller in the urban region compared to the suburban region. The average rain rate and raindrop number concentration are lower in the mountainous region compared to both urban and suburban regions. The difference in DSD between urban and suburban regions is due to the difference in DSD for the same precipitation types, while the difference in DSD between mountain and plains (i.e., urban and suburban regions) is the combined effect of the convection/stratiform ratio and the difference of DSD for the same precipitation types. Three DSD-based polarimetric radar QPE estimators were retrieved and estimated. Among these three QPE estimators, $R(Z_H)$, $R(K_{dp})$, and $R(K_{dp}, Z_{DR})$, $R(K_{dp}, Z_{DR})$ performs best, followed by $R(K_{dp})$, and $R(Z_H)$ performs worst. $R(K_{dp})$ is more sensitive to the representative parameters, while $R(Z_H)$ and $R(K_{dp}, Z_{DR})$ are more sensitive to observational error and systematic bias (i.e., calibration).

Keywords: raindrop size distribution (DSD); polarimetric radar; quantitative precipitation estimation (QPE)

Citation: Zhang, Z.; Li, H.; Li, D.; Qi, Y. Spatial Variability of Raindrop Size Distribution at Beijing City Scale and Its Implications for Polarimetric Radar QPE. *Remote Sens.* **2023**, *15*, 3964. https://doi.org/10.3390/rs15163964

Academic Editor: Kenji Nakamura

Received: 12 July 2023
Revised: 5 August 2023
Accepted: 8 August 2023
Published: 10 August 2023

1. Introduction

Raindrop size distribution (DSD) represents the combined effect of dynamic, thermodynamic, and microphysical processes in precipitation systems. Therefore, analyzing DSD is crucial for the development or validation of microphysical parameterization schemes in numerical weather prediction models [1–3], as well as for understanding the microphysical characteristics in precipitation systems [4–7], which is of great help in improving weather forecasts. DSD modeling and retrieval are also useful for improving the radar quantitative precipitation estimation (QPE) [8–10], which is critical for meteorological and hydrological applications. In addition, DSD is closely related to the kinetic energy of rain, which is critical in understanding the erosive and runoff processes of soil and the subsequent hydrological hazards [11,12].

DSD is affected by various factors, including environmental conditions (temperature, pressure, humidity, wind, aerosol, etc.), evaporation, drop sorting, clustering and breakup, and so on [5,13–15]. As a result, DSD exhibits significant variation across different climatic regimes, seasons, and precipitation types. Numerous studies have extensively investigated the characteristics of DSD worldwide, utilizing both in situ and remote sensing instruments such as radars. Bringi et al. [16] (hereinafter BR03) analyzed the DSD of convection and stratiform in different climate regimes and showed that the DSD of convection can be classified as "maritime" and "continental". Tang et al. [17] showed significant differences in DSD between the northern and southern regions of China. Other studies revealed the characteristics of DSD in different regions of China [6,18,19]. It is also found that the convection exhibits a larger mass-weighted mean diameter (D_m) and normalized intercept parameter (N_w) as compared to the stratiform [4,7,20,21]. Zeng et al. [22–24] found that both the number concentration and the drop size are larger at the top of Mt. Tianshan than at its foot.

Beijing, the capital of China with a population of over 21 million, has experienced rapid infrastructure development in recent decades. Extreme precipitation events and subsequent floods have caused great losses to the city every year. The impact of urbanization on precipitation has been widely recognized, and several possible mechanisms have been identified. These include the destabilization and perturbation of the boundary layer due to the urban heat island effect [25–27], enhanced convergence due to the large roughness in urban areas [28–30], and increased cloud condensation nuclei due to the high aerosol concentration in urban areas [31–33]. The climatological and statistical characteristics of precipitation and the mechanism of extreme precipitation systems in Beijing have been studied using rain gauges, radars, and models [34–39]. However, only a few studies have focused on the DSD characteristics in Beijing due to the lack of DSD measurements. Tang et al. [17] compared the difference in DSD characteristics between Beijing and southern China. Ji et al. [40] analyzed the DSD in Beijing based on 14-month DSD observations from one disdrometer. Ma et al. [41] studied the statistical characteristics of DSD during the rainy seasons in Beijing urban areas. These above works were only based on the observation of a single disdrometer and cannot represent the spatial variation of DSD characteristics in the whole Beijing region. As pointed out by Jaffrain et al. [42], DSD could vary even on the kilometer scale. Is there any DSD variability in different areas (urban, suburban, and mountains) of Beijing? What is the cause of the variability? These questions have not been well answered yet.

In recent years, quite a few second-generation OTT Parsivel (hereafter Parsivel^2) laser-optical disdrometers have been deployed in different areas of Beijing, providing a good opportunity to investigate the spatial variability of DSD. In this paper, we aim to reveal the DSD variability in Beijing as well as its impact on radar QPE, which would enhance our understanding of the microphysical characteristics of precipitation and improve the accuracy of radar QPE. This paper is organized as follows: Section 2 describes the data used, as well as the method for quality control, precipitation type classification, and analysis. The spatial characteristics of DSD in Beijing and its implication for polarimetric radar QPE are analyzed in Section 3. Sections 4 and 5 provide the discussion and conclusion, respectively.

2. Data and Methodology

2.1. Dataset

In this study, DSDs were collected using 11 Parsivel^2 disdrometers. The locations of these disdrometers are shown in Figure 1. In brief, Parsivel^2 is a laser-optical disdrometer that can simultaneously measure the size and falling velocity of particles. The sampling area of the Parsivel^2 is 54 cm^2 (18 cm in length and 3 cm in width). The measured size and falling velocity are divided into 32 bins. These bins are non-uniform, ranging from 0.062 to 24.5 mm for size and 0.05 to 20.8 m s^{-1} for falling velocity. Tokay et al. [43] evaluated the performance of Parsivel^2. Compared to its predecessor Parsivel, Parsivel^2 performs much better in measuring particle size, as Parsivel tends to underestimate the size of small particles and overestimate the size of large particles.

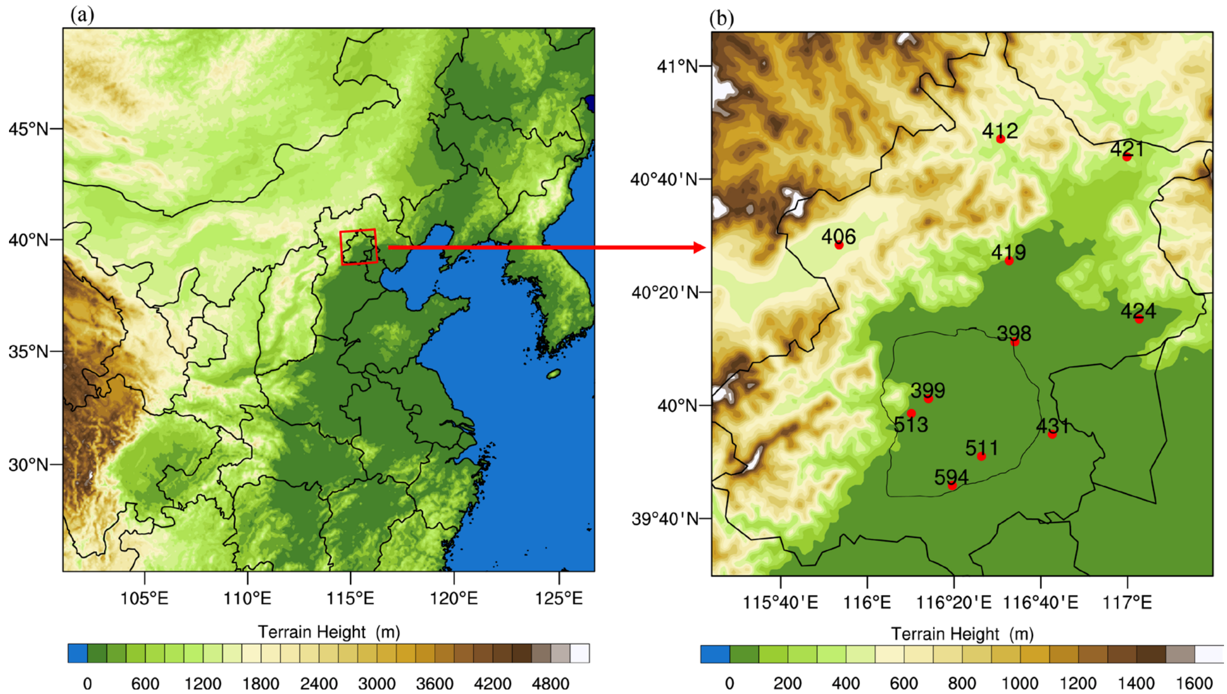

Figure 1. (**a**) Location of Beijing in China and (**b**) topography of Beijing and locations of the disdrometers used in this study. The thin black lines in (**b**) denote the 6th Ring Road of Beijing.

All the disdrometers were configured to measure DSD with a 1 min temporal resolution. The DSD data were collected from May to September 2017. Rainfall during these months accounts for 90% of the annual rainfall in Beijing.

2.2. Quality Control of DSD Dataset

Various sources affect the observational quality of the disdrometer, such as splashing of raindrops, wind effect, and margin fallers [5,13,43–46]. Therefore, quality control must be applied before using the data for analysis. The quality control procedure used here is similar to that proposed by Tokay et al. [46]. For the dataset of 1 min each, if the total drop number is less than 10, or the rain rate is less than 0.1 mm h^{-1}, this 1-min DSD is considered as noise and discarded. Drops exceeding $\pm$ 50% of their theoretical terminal falling velocity are also discarded from the DSD spectrum because such an observation may be due to splashing or wind effects. The theoretical terminal falling speed used here is based on the result of Brandes et al. [47]. The drop sizes that exceed 8 mm are also eliminated [17,41] because the largest raindrop recorded in nature are around 8 mm [48], and drops larger than 8 mm are unlikely to be raindrops.

A total number of 124,647 1-min DSD observations from 11 disdrometers passed the quality control and were used for analysis.

2.3. Separation of Precipitation Types Based on DSD Data

Previous studies have demonstrated that the characteristic DSD parameters are related to precipitation types. Therefore, it is necessary to separate different precipitation types when analyzing DSD characteristics. Numerous methods have been proposed to separate the precipitation type into convection and stratiform based on disdrometer observation [16,20,49,50]. The criteria of these methods are different, but the principles are similar: Convection usually exhibits heavier rainfall that may vary from time to time, while stratiform generally has a weaker but steadier rainfall. Therefore, when the rain rate and its variation are large, the precipitation can be classified as convection. Otherwise, it can be classified as stratiform. In this study, the precipitation separation method is similar to that of BR03. To be clear, for a 1-min DSD observation at time t, if its rain rate is greater than

5 mm h^{-1} and the standard deviation from t$-$ Δt to t+ Δt is larger than 1.5 mm h^{-1}, the DSD of this minute is classified as convection. Otherwise, it is stratiform. Δt is set to 5 min.

2.4. Raindrop Size Distribution

The direct measurement of the disdrometer provides the number of drops in each bin (i.e., i size bins and j falling velocity bins). The mid-value of each bin is taken as the representative size of the bin. The following parameters are calculated to represent the characteristics of DSD, including the total number concentration N_t, mass-weighted diameter D_m, normalized intercept parameter N_w, and rain rate R:

$$N_t = \int_{D_0}^{D_{\max}} N(D)dD \tag{1}$$

$$D_m = \int_{D_0}^{D_{\max}} D^4 N(D)dD / \int_{D_0}^{D_{\max}} D^3 N(D)dD \tag{2}$$

$$N_w = \frac{4^4}{6}\left(\int_{D_0}^{D_{\max}} D^3 N(D)dD\right)/D_m^4 \tag{3}$$

$$R = \frac{\pi}{6}\int_{D_0}^{D_{\max}} D^3 V(D)N(D)dD \tag{4}$$

where *N(D)* is the normalized number of drops in each size bin:

$$N(D) = \sum_{j=1}^{32} \frac{n_j}{A\Delta t V_j \Delta D} \tag{5}$$

where Δt, V_j, and ΔD are the measuring time, the falling velocity at a given size bin, and the size bin width, respectively. A is the effective sampling area [46]:

$$A = L(W - D_i/2) \tag{6}$$

where L and W are the length and width of the sampling area, respectively.

2.5. DSD-Based Polarimetric Radar QPE Estimators

To simulate the radar QPE of operational X-band polarimetric radars in Beijing, polarimetric radar variables are calculated from DSD data using the T-matrix method [51], including horizontal (vertical) reflectivity $Z_{\mathrm{H(V)}}$ ($\mathrm{mm^6m^{-3}}$), differential reflectivity Z_{DR}, and specific differential phase K_{dp} ($^{\mathrm{o}}\mathrm{km}^{-1}$):

$$Z_{\mathrm{H,V}} = \frac{4\lambda^4}{\pi^4|K_w|^2}\sum_{i=1}^{32}|f_{hh,vv}(180, D_i)|^2 N(D_i)\Delta D_i \tag{7}$$

$$Z_{\mathrm{DR}} = Z_{\mathrm{H}}/Z_{\mathrm{V}} \tag{8}$$

$$K_{\mathrm{dp}} = \frac{180}{\pi}\sum_{i=1}^{32}\mathrm{Re}|f_{hh}(0, D_i) - f_{vv}(0, D_i)|N(D_i)\Delta D_i \tag{9}$$

where $f_{hh,vv}(180, D_i)$ is the back scattering amplitude of horizontal and vertical polarization for a drop; $f_{hh}(0, D_i)$ and $f_{vv}(0, D_i)$ are the forward scattering amplitudes of horizontal and vertical polarization, respectively; K_w is the dielectric factor of water (0.9639) and λ is radar wavelength (32 mm in this study).

Three widely used radar estimators are applied for radar QPE:

$$R(Z_{\mathrm{H}}) = aZ_{\mathrm{H}}^{b} \tag{10}$$

$$R(K_{\mathrm{dp}}) = aK_{\mathrm{dp}}^{b} \tag{11}$$

$$R(K_{\mathrm{dp}}, Z_{\mathrm{DR}}) = aK_{\mathrm{dp}}^{b}Z_{\mathrm{DR}}^{c} \tag{12}$$

where a, b, and c are parameters.

To quantitatively evaluate the performance of different QPE estimators, 3 statistical scores are used, including the correlation coefficient (CC), root mean square error (RMSE), and relative mean bias (RMB):

$$CC = \frac{\sum_{i=1}^{n}\left(R(es)_i - \overline{R(es)}\right)\left(R(\mathrm{d})_i - \overline{R(\mathrm{d})}\right)}{\sqrt{\sum_{i=1}^{n}\left(R(es)_i - \overline{R(es)}\right)^2 \sum_{i=1}^{n}\left(R(\mathrm{d})_i - \overline{R(\mathrm{d})}\right)^2}} \tag{13}$$

$$RMSE = \left[\frac{1}{n}\sum_{i=1}^{n}\left(R(es)_i - R(\mathrm{d})_i\right)^2\right]^{1/2} \tag{14}$$

$$RMB = \sum_{i=1}^{n}\left(R(es)_i - R(\mathrm{d})_i\right) / \sum_{i=1}^{n}\left(R(\mathrm{d})_i\right) \tag{15}$$

where $R(es)_i$ is the rain rate using one of the radar estimators (i.e., Equations (10)–(12)) with radar variables simulated using DSD data with the T-matrix method (i.e., Equations (7)–(9)), and $R(\mathrm{d})_i$ is the rain rate calculated directly from the DSD data using Equation (4).

3. Results

3.1. DSD Variability in Different Areas of Beijing

The areas within the 6th Ring Road have dense infrastructure, heavy traffic, and frequent human activities. Over 90% of Beijing's population lives and works in the areas inside the 6th Ring Road, while outside the 6th Ring Road, there are mostly farms, forests, and wastelands. The topography of Beijing is characterized by plains in the center and southeast and mountains in the west and north (Figure 1). Accordingly, the 11 disdrometers used in this study were categorized into three groups based on their location: Urban stations (stations located within the 6th Ring Road, i.e., stations 399, 511, 513, and 594); suburban stations (stations located outside the 6th Ring Road with an elevation of less than 200 m above sea level, i.e., stations 398, 419, 424, and 431), and mountain stations (stations above 200 m above sea level, i.e., stations 406, 412, and 421).

The average DSD characteristics derived with all these 11 disdrometers are shown in Figure 2. Figure 2a shows the density scatter plot of D_m versus R, superimposed with the power–law relationship obtained using the least-square fit method. D_m increases with the increase in R (positive exponent in power–law relationship). As shown in the figure, D_m increases rapidly when R is less than 50 mm h^{-1}. This is because both the raindrop size and number concentration effectively increase within this rain rate range [52]. The increase in D_m becomes much slower (around 2.2~2.5 mm) when R is greater than 50 mm h^{-1}. Apparently, the increase in the rain rate mainly relies on the increase in raindrop concentration rather than raindrop size. This fact implies that the accurate estimation of particle number concentration in numerical models is crucial for better forecasting of extreme precipitation events. In addition, the spread of D_m becomes narrower with the increase in R. Such a fact suggests that when the rain rate is small, the breakup and coalescence processes of raindrops may be unbalanced, resulting in a wide spread of D_m. At a high rain rate, the breakup and coalescence are likely to reach a more balanced state. This result also explains why retrieving the rain rate using Equation (10) (traditional approach of QPE for single-polarimetric radar) is not accurate for small rain rate cases. Since parameters a and b in Equation (10) depend on DSD and there is a wide spread of DSD parameters with a small rain rate, if a fixed combination of a and b is used for QPE (the common approach for operational QPE), large errors will appear. Figure 2b is the scatter plot of D_m versus N_w for convection and stratiform in Beijing, superimposed with BR03′s results. There is a clear boundary between convection and stratiform with some overlap of samples. For convection, only 4.23% and 13.1% of the samples lie in "maritime" and "continent" clusters in BR03, respectively. The mean value point of D_m-N_w lies between these two clusters, suggesting that the characteristics of convection in Beijing be different from those places recorded in BR03. As for the stratiform, the mean value point of D_m-N_w and 90% of samples lie on the left side of the least square fitting line of stratiform in BR03, indicating that the stratiform in Beijing has a smaller raindrop size and concentration. It is notable that DSD studies in other locations of China (Nanjing, eastern China; Guangzhou and Yangjiang, southern China; Naqu, Tibet Plateau) also suggest a lower raindrop size and concentration in the stratiform as compared to BR03 [6,7,17,18].

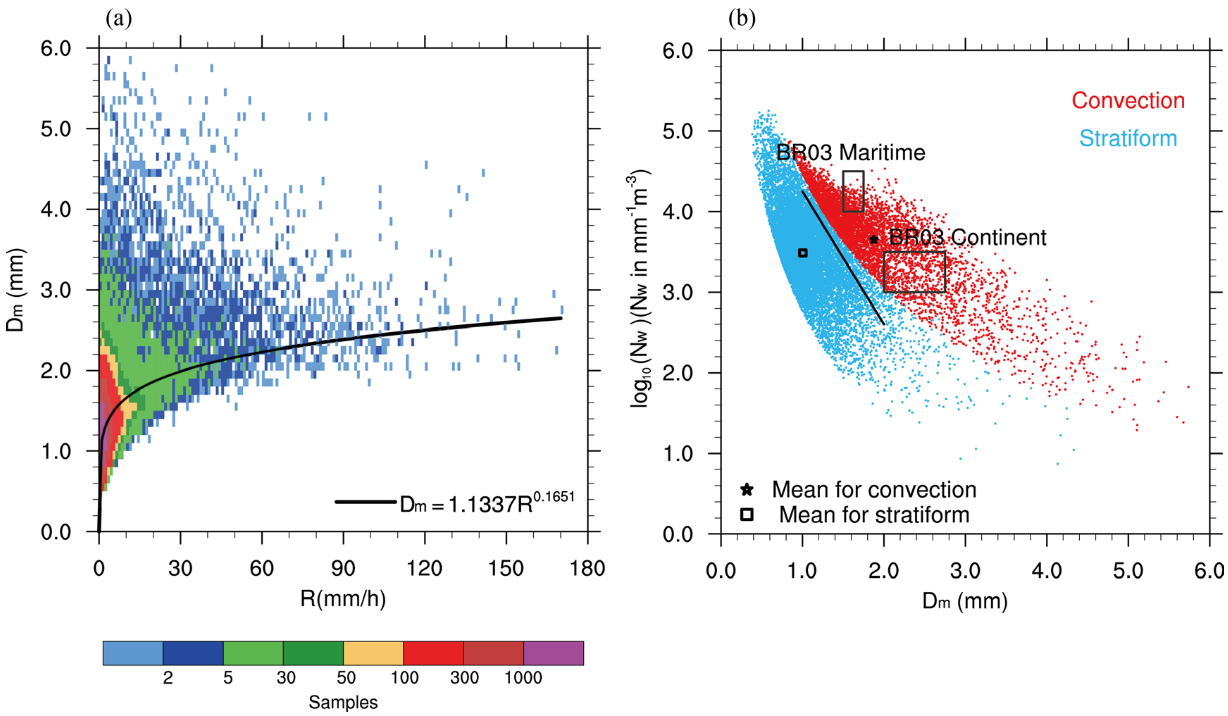

Figure 2. (**a**) Scatter density plot for R versus D_m, superimposed with the power–law relationship obtained using the least-square fit method and (**b**) scatter plot for D_m versus N_w. Red (blue) dots represent convection (stratiform). The star and square symbols represent the mean values for convection and stratiform, respectively. The black line is the log10(N_w)–D_m relationship for stratiform in BR03. Two rectangles indicate the maritime and continental convective clusters in BR03.

Figure 3 shows the variations of mean number concentration versus raindrop size in different areas of Beijing. The number concentration in mountain areas is lower than in the plains (i.e., urban and suburban areas) from the smallest raindrop size to up to 5 mm in diameter. The differences are most pronounced at the smallest sizes and around 3 mm. The urban and suburban curves are similar, but urban areas have a higher number concentration of raindrops less than 1 mm, and a lower number concentration of raindrops greater than 1 mm, indicating a smaller mean raindrop size.

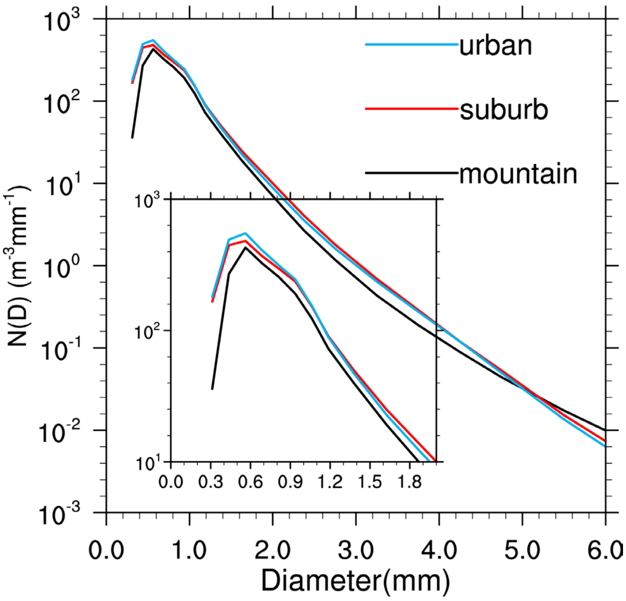

Figure 3. Average raindrop spectra for different areas of Beijing.

Table 1 shows the mean values of DSD parameters in different areas of Beijing. Among these three areas, the urban average drop size (D_m) is the smallest, and this value is comparable with previous studies based on urban disdrometer data in Beijing [40,41]. The average drop size in the suburban areas is the largest and between the two in the mountain areas. In terms of the average rain rate, the mountain areas have the smallest average rain rates, the suburban areas have the largest average rain rates, and the urban areas are in the middle. The distribution of R is consistent with previous works on the precipitation in Beijing based on rain gauge measurements [38,53,54], which found that the average hourly precipitation intensity in the mountains is smaller than that in the plains, but the total precipitation hours are larger in the mountains, mainly because light rain occurs more frequently in the mountains of Beijing. This phenomenon might be related to the specific geographical location of Beijing. The southeast flow coming from the sea is the main moisture source for precipitation systems in Beijing. The mountain areas are located in the northwest part of Beijing, which means that the mountain areas of Beijing generally receive less moisture than the plain areas of Beijing. However, although the mountain areas receive less moisture, light precipitation can easily occur when the southeast flow is elevated by the mountains. In terms of the number concentration (N_t), the mountain areas have the smallest average number concentration, the urban areas have the largest average number concentration, and the suburban areas are in the middle. In the mountain areas of Beijing, the smallest average number concentration may also be related to the frequent occurrence of light rain, as light rain is usually associated with fewer drop numbers. The comparison of these parameters in urban and suburban areas reveals that the urban environment modifies the precipitation microphysics, such that the drop size is suppressed while a greater number of drops are produced. This phenomenon may be related to the high aerosol emission in urban areas of Beijing due to human activities such as traffic. A high aerosol concentration tends to reduce the average drop size and increase the number concentration by providing more cloud condensation nuclei (CCN) [15,31,55,56].

Table 1. Mean values of DSD parameters in different areas of Beijing.

Location	Samples	D_m(mm)	R (mm h^{-1})	N_t (m^{-3})
Urban	47325	1.17	2.69	328.6
Suburb	44429	1.26	2.83	306.2
Mountain	32893	1.20	2.15	233.1

Figure 4 shows the probability distribution functions (PDF) of D_m, R, and N_t in different areas. D_m in these areas all peak around 0.9 mm, with suburban areas having the highest frequency around the peak and urban areas having the lowest (Figure 3a). The distribution of N_t in the mountain areas is sharper and more symmetrical compared to those in the plains (i.e., urban and suburban areas). Both the urban and suburban areas have a broader distribution around the peak, and the frequency decreases faster toward the higher N_t end than toward the lower N_t end. In addition, urban areas have a higher distribution for N_t larger than 10^3 and a lower distribution for N_t from 10^2 to $10^{2.5}$. As for the PDF for R, R less than $10^{0.5}$ mm h^{-1} is mainly responsible for the differences in different areas. There is a sharper and higher peak in mountain areas at the lower end of R, indicating that light rain occurs more frequently in mountain areas than in plains. There is a higher frequency of rain rate from 10^0 to $10^{0.5}$ and larger than $10^{1.0}$ mm h^{-1} in plains than in mountain areas, while the rain rate from $10^{0.5}$–$10^{1.0}$ is quite close together. This result suggests that the mountains in Beijing may play a role in modifying precipitation microphysics mainly for precipitation with a rain rate less than $10^{0.5}$ or larger than $10^{1.0}$ mm h^{-1}. Light rain occurs more frequently in mountain areas because mountain areas receive less moisture than the plains in Beijing as the southeast wet flow travels further to reach the mountain areas in the western part of Beijing [38,53,54]. As for the differences between urban and suburban areas, suburban areas have a high frequency of rain rate of less than $10^{0.3}$ mm h^{-1} and more than $10^{1.3}$ mm h^{-1}, with a lower frequency in the middle.

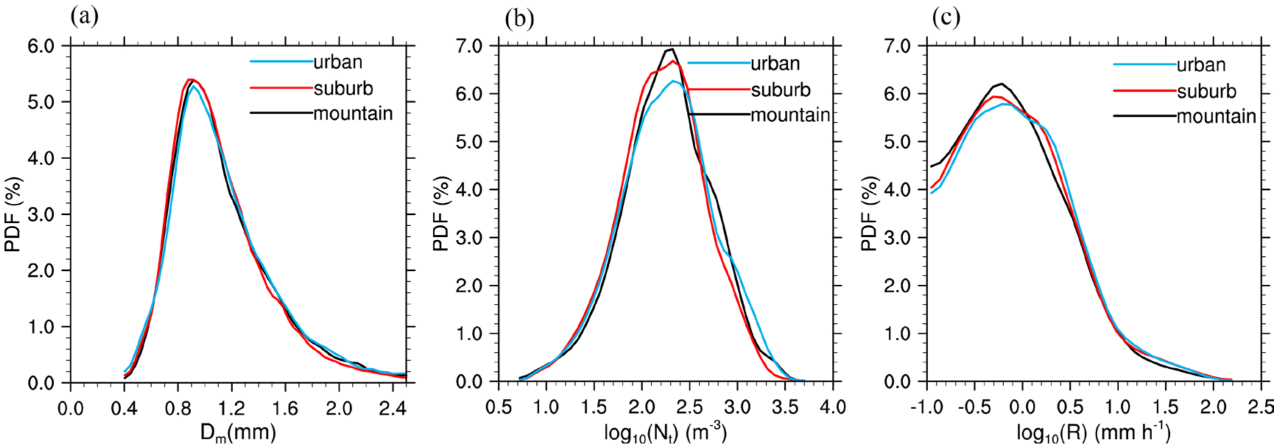

Figure 4. The probability distribution functions (PDF) of (**a**) D_m, (**b**) N_t, and (**c**) R for different areas of Beijing.

Numerous studies have shown that D_m, R, and N_t are larger in convection than in stratiform [16,17,20], and other studies suggested that the terrain or urban environments can modify the microphysics processes in precipitation systems and change the DSD characteristics [24,57]. Consequently, there might be three causes responsible for the variation in DSD characteristics in different regions of Beijing: (1) The ratio of convection/stratiform might be different in different regions and the higher frequency of convection might lead to larger D_m, R, and N_t; (2) for the same precipitation type, DSD characteristics in different regions might be different due to the terrain or urban effect; or (3) the combination of (1) and (2).

Accordingly, DSD observations were classified into convection and stratiform for further analysis. The DSD parameters, number of samples, and percentage of convection and stratiform in different areas of Beijing are shown in Table 2. First, the difference between urban and suburban areas was analyzed. Although the average D_m is larger in suburban areas than that in urban areas, it is surprising to see that the percentage of convection in suburban areas is almost identical to that in urban areas (8.58% versus 8.60%). Consequently, the differences in D_m between urban and suburban areas are not likely due to differences in convection/stratiform ratios but rather are more likely due to differences in DSD characteristics for the same precipitation type. For both convection and stratiform, D_m is smaller in urban areas than in suburban areas, perhaps due to the high aerosol concentration in urban areas of Beijing. High aerosol concentration usually causes smaller raindrop sizes by providing high CCN [15]. A study on the spatial distribution of PM2.5 (particulate matter with aerodynamic diameters of less than 2.5 μm) in Beijing shows that the PM2.5 concentration is much higher in urban areas than in suburbs during rainy seasons [58]. On the other hand, smaller raindrops tend to evaporate more quickly after falling out of the cloud, which may further lead to smaller raindrops in urban areas. Urban areas have smaller R and N_t for convection than suburban areas, but larger ones for stratiform. The result suggests urbanization affects convection and stratiform differently, whereby the urban environment tends to reduce the intensity of rain and the number concentration of raindrops in convection while positively influencing them in stratiform. It appears that the differences in DSD between urban areas and suburban areas are not due to differences in convection/stratiform ratios, but rather due to differences in DSD characteristics for the same precipitation types.

Table 2. Mean values of DSD parameters, number of samples, and percentage of convection and stratiform in different areas of Beijing.

Location	Precipitation Type	Samples	Percentage (%)	D_m(mm)	R (mm h^{-1})	N_t (m^{-3})
Urban	convection	4070	8.60	1.85	18.25	863.4
	stratiform	43,255	91.40	0.97	1.22	278.3
Suburb	convection	3810	8.58	1.92	20.29	949.8
	stratiform	40,619	91.42	1.02	1.20	245.7
Mountain	convection	2149	6.53	1.85	16.93	681.3
	stratiform	30,744	93.47	1.05	1.11	201.7

The convection/stratiform ratio in mountain areas is lower than that in the plains, and only 6.53% of the total precipitation is convection. For convection, D_m in mountain areas is almost the same as that in urban areas and smaller than that in suburban areas. However, for stratiform, D_m in mountain areas is larger than that in the plains. R and N_t for both convection and stratiform are smaller in mountain areas than in the plains. Therefore, smaller R and N_t values in mountain areas are the combined result of a smaller convection/stratiform ratio and smaller R and N_t values for the same precipitation types. Such a result may be related to the moisture conditions in Beijing. Beijing typically receives its moisture from the east (from the ocean), which travels hundreds of kilometers before reaching Beijing (the nearest ocean is 160 km away). The mountain areas on the west side of Beijing receive less moisture than the plain areas on the east, thereby reducing convection frequency, rain intensity, and number concentration.

3.2. Implication for QPE of Polarimetric Radar

Several X-band polarimetric radars (λ = 3.2 cm) have been deployed in Beijing in recent years, aiming at providing better QPE products to meet the needs of meteorological and hydrological applications. These radars all operate in VCP 21 mode, which completes a volume scan in 3 min with radial and azimuth resolutions of 75 m and 0.95°, respectively. To study the X-band radar QPE using DSD data, the polarimetric radar variables of Z_H, Z_{DR}, and K_{dp} were calculated from 1 min DSD observations. The parameters of a, b, and c in Equations (10)–(12) were then derived using the nonlinear least square fitting. The fitted parameters using DSD data collected in all locations, namely, urban, suburban, and mountain areas, are listed in Table 3. As Table 3 shows, these parameters vary in different regions of Beijing due to the DSD variability.

Table 3. The fitted parameters for QPE estimators.

Estimator	Location	a	b	c
R(Z_H)	Entire	0.1232	0.4758	\
	Urban	0.1243	0.4756	\
	Suburb	0.107	0.4927	\
	Mountain	0.1203	0.4646	\
R(K_{dp})	Entire	15.83	0.7727	\
	Urban	15.87	0.7721	\
	Suburb	15.97	0.8078	\
	Mountain	14.99	0.7277	\
R(K_{dp}, Z_{DR})	Entire	30.31	0.9676	−1.409
	Urban	29.17	0.9554	−1.309
	Suburb	29.78	0.9856	−1.38
	Mountain	30.04	0.9324	−1.431

Figure 5 illustrates the scatter density plots of R estimated from four estimators (Table 3) versus R calculated directly from the 1 min DSD data. The statistical values of CC, RMSE and RMB are also shown. As shown in Figure 5, the estimator R(Z_H) performs the worst (Figure 5a) with the smallest CC and largest RMSE and RMB. The uncertainty of QPE increases greatly with the intensity of R. The difference between $R(es)_i$ and $R(\mathrm{d})_i$ can be up to approximately 4 times (e.g., 30 mm h^{-1} of $R(es)_i$ versus 120 mm h^{-1} of $R(\mathrm{d})_i$). When polarimetric variables of Z_{DR} and K_{dp} are introduced, the accuracy of QPE is much better (Figure 5b–c). Among these three estimators, R(K_{dp}, Z_{DR}) performs the best, providing the most accurate estimation for light rain to heavy rain.

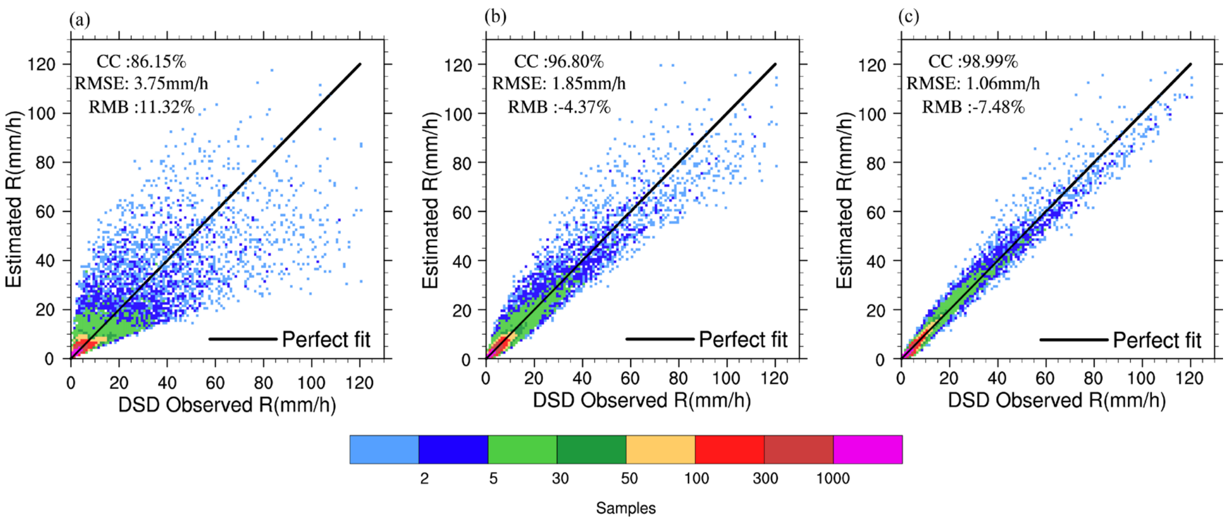

Figure 5. Scatter density plots of R from all 11 disdrometer observations and R estimated using estimators: (**a**) R(Z_H), (**b**) R(K_{dp}), and (**c**) R(K_{dp}, Z_{DR}). The black line in each panel is the perfect fit line (i.e., y = x). Statistical scores of CC, RMSE, and RMB are superimposed.

The results shown in Figure 5 can be regarded as the theoretical upper limit of the performances of the estimators. When performing QPE estimators into operational radar, three aspects below affect the accuracy of the QPE result: Random observational errors of the radar variables, the systematic bias of the radar variables due to miscalibration, and the variability of the parameters of the QPE estimators due to DSD variability. It is well-known that the DSD variability in different climate regions significantly affects QPE accuracy. However, for city scales such as Beijing, it is unclear how much the DSD variability affects the QPE accuracy compared to radar variables measurement errors and bias. What is the dominant source of error for QPE? To find the answer, a series of experiments were performed using these DSD data.

The actual distribution of radar observational errors can be very complicated. However, for ideal experiments using DSD data, let us assume that the errors conform to the most general type of error distribution, the normal distribution $N(\mu, \sigma^2)$, where μ and σ are the mean value and standard deviation. Approximately 68% and 95% of the total samples lie between $\mu - \sigma$ to $\mu + \sigma$ and $\mu - 2\sigma$ to $\mu + 2\sigma$, respectively. Assuming that the radar observational variables follow the normal distribution, then the observational variables can be perturbed by multiplying $N(\mu, \sigma^2)$ to simulate measurement errors and systematic bias. For example, $Z'_h = Z_h \bullet N(1, 0.15^2)$ means measurement errors exist in Z_h, while approximately 95% of the measured Z_h are between 0.7 and 1.3 times the theoretical Z_h; $Z'_h = Z_h \bullet N(1.05, 0.15^2)$ means both measurement errors and systematic bias exist in Z_h, the mean observational Z_h is stronger for 5% than the theoretical Z_h, and approximately 95% of the measured Z_h are between 0.75 to 1.35 time of the theoretical Z_h.

Table 4 shows the experiment design of R(Z_H). All the DSD data collected by these 11 disdrometers are used in these experiments. In the control experiment, the rain rate is estimated using parameters obtained for the whole region of Beijing; it is the theoretical upper limit capability of applying R(Z_H) to perform QPE. In the DSD variability experiment, the rain rate is estimated using parameters obtained for the mountain region of Beijing. The purpose of this experiment is to find out how much the DSD variability can affect the accuracy of QPE when the parameters for specific regions (e.g., mountains) are used to estimate the rain rate for the whole region of Beijing. In the measurement error experiment, the Z_h is perturbed by multiplying $N(1, 0.05^2)$. This experiment aims to find out if there are measurement errors of Z_h between operational radar and disdrometer and how much the error can affect the accuracy of QPE. Furthermore, the systematic bias experiment is designed to find out how much the error and systematic bias (i.e., calibration issues) can affect the accuracy of QPE, and which of these above issues affect the accuracy of QPE the most.

Table 4. Experiment design of R(Z_H) estimator.

Name	Description
Control experiment	Perform R(Z_H) to estimate rain rate using all the DSD data with parameters for the whole region of Beijing (i.e., a = 0.1232 and b = 0.4758)
DSD variability experiment	Perform R(Z_H) to estimate rain rate using all the DSD data with parameters for the mountain region of Beijing (i.e., a = 0.1202 and b = 0.4646)
Measurement error experiment	Perturb Z_h by multiplying $N(1, 0.05^2)$
Systematic bias experiment	Perturb Z_h by multiplying $N(1.05, 0.05^2)$

Figure 6 shows the results of the R(Z_H) experiment. If inappropriate parameter values (DSD variability experiment, Figure 6b) are used in QPE, such as using the parameters obtained in the mountain area to estimate the rain rate for the entire region of Beijing, it will lead to systematic bias in QPE. In this case, the rain rate is underestimated, as can be seen in Figure 6b, where more dots appear in the lower right part. The RMSE does not change much, with the RMSE increasing from 3.75 mm h^{-1} to 3.88 mm h^{-1}, and an even higher CC. The measurement errors affect the accuracy of QPE more significantly, as shown in Figure 6c; even if 95% of the observational Z_h are within 10% measurement errors, the QPE accuracy drops significantly, especially for heavy precipitation. With a rain rate larger than 50 mm h^{-1}, the dots become much more scattered than in Figure 6a, and RMSE rises to 4.23 mm h^{-1}. When both measurement errors and systematic bias of Z_h coexist, as shown in Figure 6d, the QPE accuracy decreases even more. The QPE overestimates the rain rate by 38.82%, with more dots appearing in the upper right part and becoming more scattered, and the RMSE increases significantly to 5.26 mm h^{-1}. This result suggests that for a city-scale region such as Beijing, when R(Z_H) is used for QPE, the variability of DSD certainly affects the QPE accuracy, but the main influencing factors on QPE accuracy are the measurement errors and calibration of reflectivity, and they affect the QPE accuracy to a greater extent than the influence of the variability of DSD. Therefore, we should focus more on improving the quality of the reflectivity when utilizing R(Z_H) in operation.

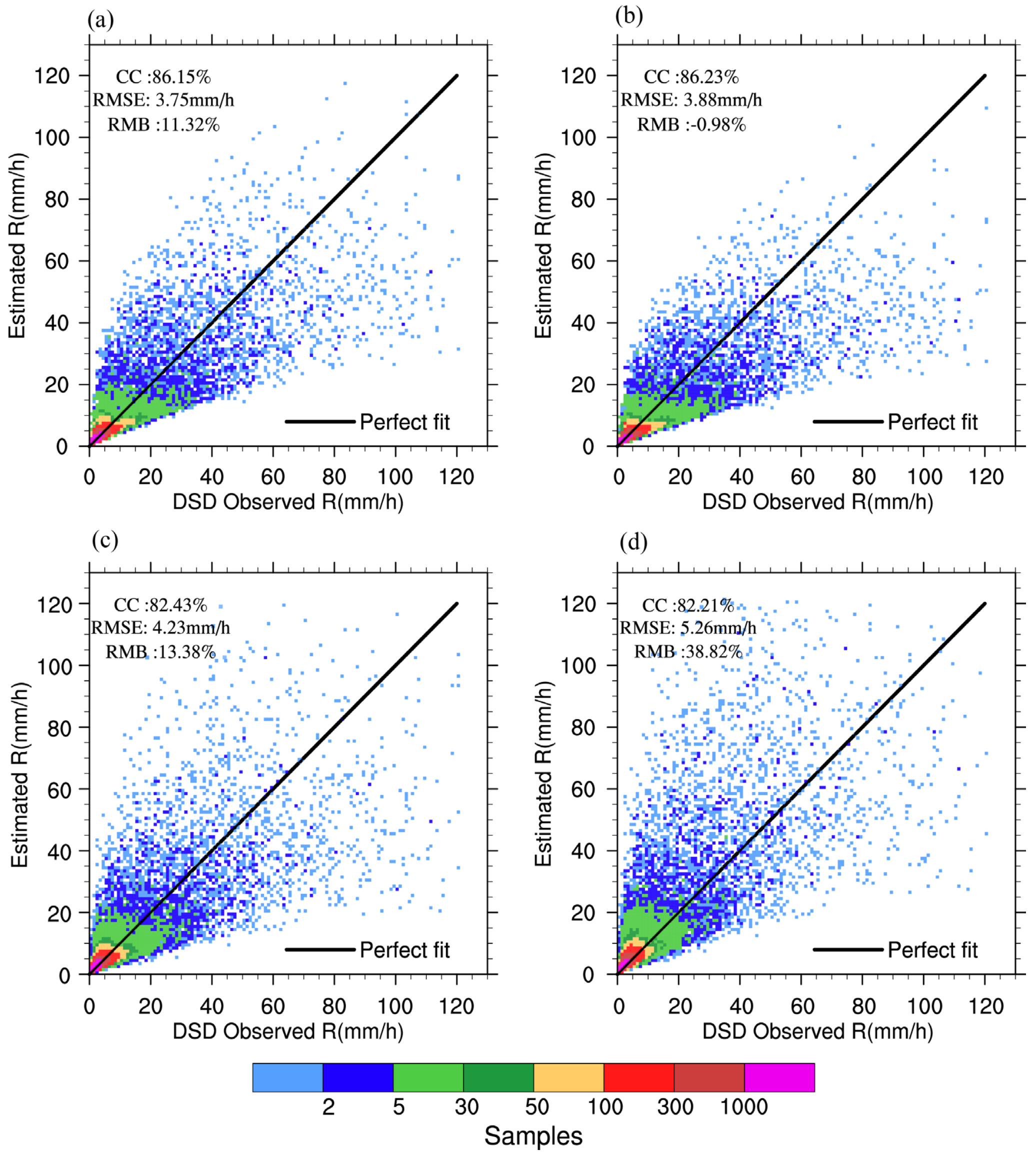

Figure 6. Scatter density plots of R in the whole region of Beijing from 11 disdrometer observations and R estimated using estimator R(Z_H): (**a**) Control experiment, (**b**) DSD variability experiment, (**c**) measurement error experiment, and (**d**) systematic bias experiment as described in Table 4. The black line in each panel is the perfect fit line (i.e., y = x). Statistical scores of CC, RMSE, and RMB are superimposed.

Similarly, the experiment design of R(K_{dp}) is shown in Table 5. Since K_{dp} is immune to calibration, the systematic bias experiment was discarded, and an additional measurement error experiment was added. The results are shown in Figure 7. Some previous works have suggested that the R(K_{dp}) estimator is relatively insensitive to the variability of DSD compared to R(Z_H) [47,59,60], but by comparing Figure 7a,b, it is clear that the variability of DSD does affect the accuracy of QPE using R(K_{dp}), at least for heavy precipitation. In this case, using parameters for the mountain region to estimate the rain rate for the entire region of Beijing results in the underestimation of heavy precipitation, as shown in Figure 7b. More dots with a rain rate larger than 50 mm h^{-1} appear in the lower right flank of the perfect line. The measurement errors, on the other hand, do not significantly affect the accuracy of QPE. Perturbing K_{dp} by multiplying $N(1, 0.05^2)$ does not degrade the performance much (Figure 7c), with CC, RMSE, and RMB quite close to the control experiment. Even when perturbing K_{dp} by multiplying $N(1, 0.15^2)$, which means assuming large measurement errors for K_{dp} (approximately 32% of the K_{dp} observation errors are larger than 15%), the QPE accuracy does not deteriorate significantly (Figure 7d), and it is comparable to the result of Figure 7b. This series of experiments on R(K_{dp}) suggest that the variability of DSD even at the city scale could lead to systematic bias in QPE, especially for heavy precipitation. The variability of DSD may affect the accuracy of QPE even more than K_{dp} measurement errors. Therefore, when utilizing R(K_{dp}) to perform QPE in operational usage, special attention should be paid to obtaining appropriate parameters.

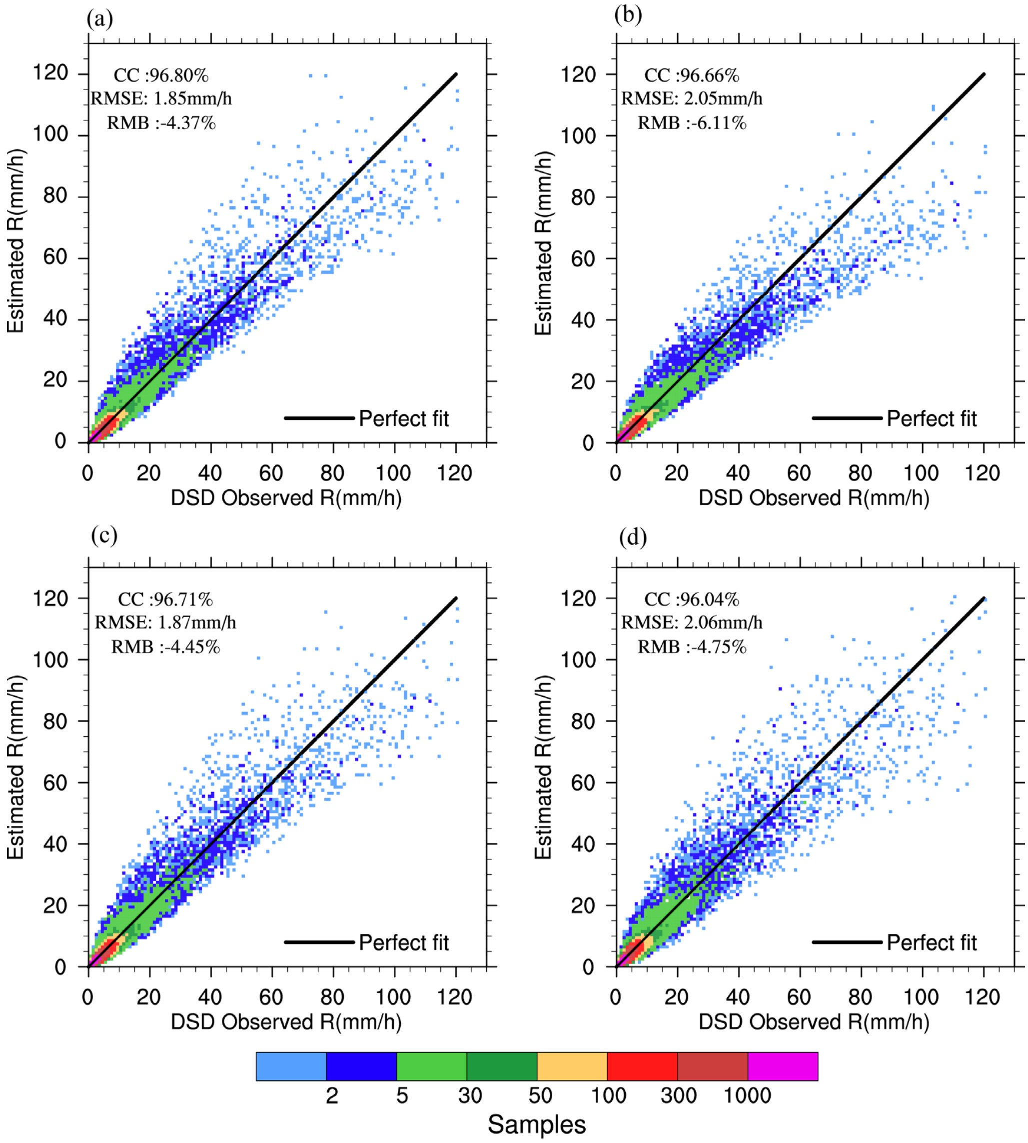

Figure 7. Scatter density plots of R in the whole region of Beijing from 11 disdrometer observations and R estimated using estimator R(K_{dp}): (**a**) Control experiment, (**b**) DSD variability experiment, (**c**) measurement error experiment 1, and (**d**) measurement error experiment 2 as described in Table 5. The black line in each panel is the perfect fit line (i.e., y = x). Statistical scores of CC, RMSE, and RMB are superimposed.

Table 5. Experiment design of R(K_{dp}) estimator.

Name	Description
Control experiment	Perform R(K_{dp}) to estimate rain rate using all the DSD data with parameters for the whole region of Beijing (i.e., a = 15.83 and b = 0.7727)
DSD variability experiment	Perform R(K_{dp}) to estimate rain rate using all the DSD data with parameters for the mountain region of Beijing (i.e., a = 14.99 and b = 0.7727)
Measurement error experiment 1	Perturb K_{dp} by multiplying $N(1, 0.05^2)$
Measurement error experiment 2	Perturb K_{dp} by multiplying $N(1, 0.15^2)$

Experiments on R(K_{dp}, Z_{DR}) are also performed using the design outlined in Table 6, and the results are shown in Figure 8. Similar to the R(K_{dp}) experiment, although R(K_{dp}, Z_{DR}) is relatively insensitive to the variability of DSD, the variability of DSD does affect the accuracy of R(K_{dp}, Z_{DR}), at least for heavy precipitation above 50 mm h^{-1}. As shown in Figure 8b, R(K_{dp}, Z_{DR}) underestimates heavy precipitation above 50 mm h^{-1} when inappropriate parameters are used. When Z_{DR} is assumed to have observational errors (Figure 8c), the accuracy of QPE drops significantly, especially for heavy precipitation above 50 mm h^{-1}, resulting in more scattered dots. When both observational errors and systematic bias coexist (Figure 8d), the accuracy of QPE becomes worse. In this case, the QPE systematically overestimates the rain rate, with more dots appearing in the upper left flank of the perfect line, and the dots become more scattered. These results suggest that the accuracy of R(K_{dp}, Z_{DR}) may be more sensitive to observational errors and systematic bias rather than the representative parameters. It could be due to the negative parameter c, which puts ZDR in the denominator. Given that Z_{DR} is small in rain (generally less than 3 dB), a small fluctuation or deviation of Z_{DR} may lead to significant errors in QPE. Therefore, accurate Z_{DR} observation is crucial to the QPE accuracy for R(K_{dp}, Z_{DR}) estimator. Therefore, accurate and well-calibrated Z_{DR} observations are crucial to ensure the accuracy of QPE using the R(K_{dp}, Z_{DR}) estimator. Introducing Z_{DR} into QPE may not necessarily have a positive impact, but rather a negative impact on QPE accuracy if Z_{DR} is not measured accurately and well-calibrated.

Table 6. Experiment design of R(K_{dp}, Z_{DR}) estimator.

Name	Description
Control experiment	Perform R(K_{dp}, Z_{DR}) to estimate rain rate using all the DSD data with parameters for the whole region of Beijing(i.e., a = 30.31, b = 0.9676, and c = −1.409)
DSD variability experiment	Perform R(K_{dp}, Z_{DR}) estimate rain rate using all the DSD data with parameters for the mountain region of Beijing(i.e., a = 30.04, b = 0.9324, and c = −1.431)
Measurement error experiment	Perturb Z_{DR} by multiplying $N(1, 0.10^2)$
Systematic bias experiment	Perturb Z_{DR} multiplying $N(0.95, 0.1^2)$

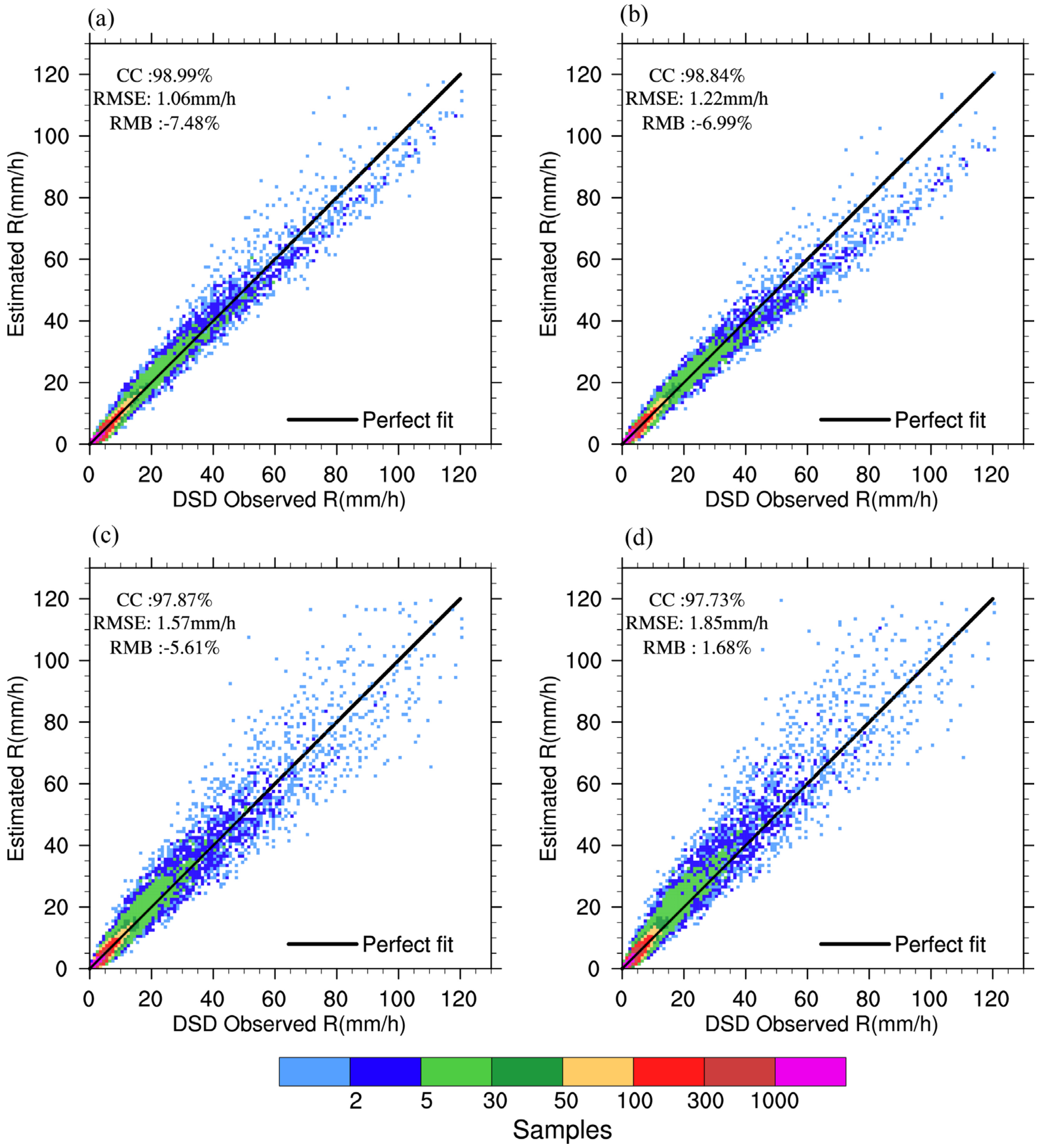

Figure 8. Scatter density plots of R in the whole region of Beijing from 11 disdrometer observations and R estimated using estimator R(K_{dp},Z_{dr}): (**a**) Control experiment, (**b**) DSD variability experiment, (**c**) measurement error experiment, and (**d**) systematic bias experiment as described in Table 6. The black line in each panel is the perfect fit line (i.e., y = x). Statistical scores of CC, RMSE, and RMB are superimposed.

4. Discussion

In this study, disdrometer data collected from 11 sites in Beijing in 2017 are analyzed to reveal the city-scale spatial variability of DSD, and to investigate its impact on radar QPE. We found that the average precipitation intensity is smaller in the mountain areas of Beijing and more light rain occurs. It should be pointed out that this phenomenon is only specific to the mountain areas of Beijing, not worldwide. This phenomenon is possible due to the specific location of Beijing, that is, the mountain areas are further away from the sea and receive less moisture than the plains in Beijing. As for other places, some previous studies suggested that the mountains tend to enhance the precipitation [24,61]. A series of sensitivity experiments were conducted to investigate the effect of DSD variability on radar QPE. However, it should be pointed out that these experiments are ideal experiments based on DSD data and no real radar data are used yet. Utilizing real radar data to perform QPE is more complicated, and the errors of radar observation may not simply conform to a Gaussian distribution. In addition, the disdrometer measures DSD information at ground level while the weather radar measures microwave electromagnetic scattering of precipitation particles in the air. These two types of instruments do not measure precipitation at the same location, and the sampling volumes of these two types of instruments are also different, with the sampling volume of weather radar being much larger. This work provides insights into the relative importance of the factors that affect the accuracy of QPE with sensitivity experiments, and more work needs to be performed when applying these results to the operational usage of weather radar.

5. Conclusions

In this study, disdrometer data collected from 11 sites in Beijing in 2017 are analyzed to reveal the variability of DSD and to investigate its impact on radar QPE. The main conclusions are summarized as follows:

DSD exhibits evidently different characteristics in urban, suburban, and mountain areas of Beijing. Specifically, the average raindrop diameter is smaller in the urban area compared to the suburban area. Additionally, the average rain rate and raindrop number concentration are lower in mountain areas compared to both urban and suburban areas.

The convection/stratiform ratio is almost the same in urban and suburban areas, indicating that the difference in DSD between urban and suburban areas is due to the difference in DSD within the same precipitation types. In the urban area, both convection and stratiform exhibit smaller average raindrop diameters compared to the suburban area. This difference may be attributed to higher aerosol concentrations in the urban area.

The lower average rain rate and raindrop number concentration in mountain areas is the combined effect of the convection/stratiform ratio and the DSD difference for the same precipitation types. Convection occurs less frequently in mountain areas, and the rain rate and raindrop number concentration are also smaller both for convection and stratiform, resulting in the smaller average rain rate and raindrop number concentration in mountain areas.

Among the three QPE estimators of $R(Z_H)$, $R(K_{dp})$, and $R(K_{dp}, Z_{DR})$, $R(K_{dp}, Z_{DR})$ performs best, followed by $R(K_{dp})$, and $R(Z_H)$ performs worst. The $R(K_{dp})$ is more sensitive to the representative parameters while $R(Z_H)$ and $R(K_{dp}, Z_{DR})$ are more sensitive to the observational error and systematic bias (i.e., calibration).

Our conclusions suggest that when performing QPE at the city scale using different QPE estimators, special attention should be paid to different aspects to improve the accuracy of QPE. However, these results are based on DSD data and sensitivity experiments, and it should be noted that this conclusion needs to be further confirmed by using polarimetric radar data in the future. In addition, there are also other factors that influence the operational radar QPE, such as beam blockage by terrains, the undersampling of the disdrometer, and the variation in DSD when raindrops are falling in the air (where the radar samples them) and on the ground (where the disdrometer samples them). Moreover, for other regions such as Southwest China where there are many mountains, how these mountains affect the DSD variability is worth studying. All of these issues are crucial to obtaining accurate QPE and will be further studied in future work.

Author Contributions: Conceptualization, Z.Z. and H.L.; data curation, D.L. and Y.Q.; formal analysis, Z.Z., H.L. and Y.Q.; methodology, Z.Z. and H.L. supervision, D.L. and Y.Q.; writing— original draft, Z.Z.; writing— review and editing, Z.Z., H.L. and Y.Q. All authors have read and agreed to the published version of the manuscript.

Funding: This research was funded by the National Key Research and Development Program of China (2022YFC3003902 and 2022YFC3002904), and National Natural Science Foundation of China (41905047).

Data Availability Statement: Not applicable.

Acknowledgments: The authors would like to thank the editors and the reviewers for their thorough comments, which really helped improve the manuscript.

Conflicts of Interest: The authors declare no conflict of interest.

References

1. Milbrandt, J.; Yau, M. A multimoment bulk microphysics parameterization. Part I: Analysis of the role of the spectral shape parameter. *J. Atmos. Sci.* **2005**, *62*, 3051–3064. [CrossRef]
2. Morrison, H.; Curry, J.; Khvorostyanov, V. A new double-moment microphysics parameterization for application in cloud and climate models. Part I: Description. *J. Atmos. Sci.* **2005**, *62*, 1665–1677. [CrossRef]
3. Zhang, G.; Sun, J.; Brandes, E.A. Improving parameterization of rain microphysics with disdrometer and radar observations. *J. Atmos. Sci.* **2006**, *63*, 1273–1290. [CrossRef]
4. Maki, M.; Keenan, T.D.; Sasaki, Y.; Nakamura, K. Characteristics of the Raindrop Size Distribution in Tropical Continental Squall Lines Observed in Darwin, Australia. *J. Appl. Meteorol.* **2001**, *40*, 1393–1412. [CrossRef]
5. Cao, Q.; Zhang, G.; Brandes, E.; Schuur, T.; Ryzhkov, A.; Ikeda, K. Analysis of video disdrometer and polarimetric radar data to characterize rain microphysics in Oklahoma. *J. Appl. Meteorol. Climatol.* **2008**, *47*, 2238–2255. [CrossRef]
6. Wen, L.; Zhao, K.; Zhang, G.; Xue, M.; Zhou, B.; Liu, S.; Chen, X. Statistical characteristics of raindrop size distributions observed in East China during the Asian summer monsoon season using 2-D video disdrometer and Micro Rain Radar data. *J. Geophys. Res. Atmos.* **2016**, *121*, 2265–2282. [CrossRef]
7. Wang, H.; Kong, F.; Wu, N.; Lan, H.; Yin, J. An investigation into microphysical structure of a squall line in South China observed with a polarimetric radar and a disdrometer. *Atmos. Res.* **2019**, *226*, 171–180. [CrossRef]
8. Zhang, G.; Vivekanandan, J.; Brandes, E. A method for estimating rain rate and drop size distribution from polarimetric radar measurements. *IEEE Trans. Geosci. Remote Sens.* **2001**, *39*, 830–841. [CrossRef]
9. Cao, Q.; Zhang, G.; Brandes, E.A.; Schuur, T.J. Polarimetric radar rain estimation through retrieval of drop size distribution using a Bayesian approach. *J. Appl. Meteorol. Climatol.* **2010**, *49*, 973–990. [CrossRef]
10. Chen, G.; Zhao, K.; Zhang, G.; Huang, H.; Liu, S.; Wen, L.; Yang, Z.; Yang, Z.; Xu, L.; Zhu, W. Improving Polarimetric C-Band Radar Rainfall Estimation with Two-Dimensional Video Disdrometer Observations in Eastern China. *J. Hydrometeorol.* **2017**, *18*, 1375–1391. [CrossRef]
11. Angulo-Martínez, M.; Barros, A. Measurement uncertainty in rainfall kinetic energy and intensity relationships for soil erosion studies: An evaluation using PARSIVEL disdrometers in the Southern Appalachian Mountains. *Geomorphology* **2015**, *228*, 28–40. [CrossRef]
12. Caracciolo, C.; Napoli, M.; Porcù, F.; Prodi, F.; Dietrich, S.; Zanchi, C.; Orlandini, S. Raindrop size distribution and soil erosion. *J. Irrig. Drain. Eng.* **2012**, *138*, 461–469. [CrossRef]
13. Friedrich, K.; Higgins, S.; Masters, F.J.; Lopez, C.R. Articulating and stationary PARSIVEL disdrometer measurements in conditions with strong winds and heavy rainfall. *J. Atmos. Ocean. Technol.* **2013**, *30*, 2063–2080. [CrossRef]
14. May, P.T.; Bringi, V.N.; Thurai, M. Do We Observe Aerosol Impacts on DSDs in Strongly Forced Tropical Thunderstorms. *J. Atmos. Sci.* **2011**, *68*, 1902–1910. [CrossRef]
15. Tao, W.; Chen, J.; Li, Z.; Wang, C.; Zhang, C. Impact of aerosols on convective clouds and precipitation. *Rev. Geophys.* **2012**, *50*, RG2001. [CrossRef]
16. Bringi, V.; Chandrasekar, V.; Hubbert, J.; Gorgucci, E.; Randeu, W.; Schoenhuber, M. Raindrop size distribution in different climatic regimes from disdrometer and dual-polarized radar analysis. *J. Atmos. Sci.* **2003**, *60*, 354–365. [CrossRef]
17. Tang, Q.; Xiao, H.; Guo, C.; Feng, L. Characteristics of the raindrop size distributions and their retrieved polarimetric radar parameters in northern and southern China. *Atmos. Res.* **2014**, *135*, 59–75. [CrossRef]
18. Chen, B.; Hu, Z.; Liu, L.; Zhang, G. Raindrop Size Distribution Measurements at 4500 m on the Tibetan Plateau During TIPEX-III. *J. Geophys. Res. Atmos.* **2017**, *122*, 11092–11106. [CrossRef]
19. Niu, S.; Jia, X.; Sang, J.; Liu, X.; Lu, C.; Liu, Y. Distributions of raindrop sizes and fall velocities in a semiarid plateau climate: Convective versus stratiform rains. *J. Appl. Meteorol. Climatol.* **2010**, *49*, 632–645. [CrossRef]
20. Chen, B.; Yang, J.; Pu, J. Statistical characteristics of raindrop size distribution in the Meiyu season observed in eastern China. *J. Meteorol. Soc. Japan. Ser. II* **2013**, *91*, 215–227. [CrossRef]
21. Luo, L.; Xiao, H.; Yang, H.; Chen, H.; Guo, J.; Sun, Y.; Feng, L. Raindrop size distribution and microphysical characteristics of a great rainstorm in 2016 in Beijing, China. *Atmos. Res.* **2020**, *239*, 104895. [CrossRef]
22. Zeng, Y.; Tong, Z.; Jiang, Y.; Zhou, Y. Microphysical characteristics of seasonal rainfall observed by a Parsivel disdrometer in the Tianshan Mountains, China. *Atmos. Res.* **2022**, *280*, 106459. [CrossRef]
23. Zeng, Y.; Yang, L.; Tong, Z.; Jiang, Y.; Chen, P.; Zhou, Y. Characteristics and Applications of Summer Season Raindrop Size Distributions Based on a PARSIVEL2 Disdrometer in the Western Tianshan Mountains (China). *Remote Sens.* **2022**, *14*, 3988. [CrossRef]
24. Zeng, Y.; Yang, L.; Zhou, Y.; Tong, Z.; Jiang, Y.; Chen, P. Characteristics of orographic raindrop size distribution in the Tianshan Mountains, China. *Atmos. Res.* **2022**, *278*, 106332. [CrossRef]

25. Baik, J.; Kim, Y.; Chun, H. Dry and Moist Convection Forced by an Urban Heat Island. *J. Appl. Meteorol.* **2001**, *40*, 1462–1475. [CrossRef]
26. Shepherd, J.M.; Burian, S.J. Detection of Urban-Induced Rainfall Anomalies in a Major Coastal City. *Earth Interact.* **2003**, *7*, 1–17. [CrossRef]
27. Zhong, S.; Qian, Y.; Zhao, C.; Leung, R.; Wang, H.; Yang, B.; Fan, J.; Yan, H.; Yang, X.; Liu, D. Urbanization-induced urban heat island and aerosol effects on climate extremes in the Yangtze River Delta region of China. *Atmos. Chem. Phys.* **2016**, *17*, 5439–5457. [CrossRef]
28. Bornstein, R.; Lin, Q. Urban heat islands and summertime convective thunderstorms in Atlanta: Three case studies. *Atmos. Environ.* **2000**, *34*, 507–516. [CrossRef]
29. Guo, X.; Fu, D.; Wang, J. Mesoscale convective precipitation system modified by urbanization in Beijing City. *Atmos. Res.* **2006**, *82*, 112–126. [CrossRef]
30. Han, J.-Y.; Baik, J.-J.; Lee, H. Urban impacts on precipitation. *Asia-Pac. J. Atmos. Sci.* **2014**, *50*, 17–30. [CrossRef]
31. Rosenfeld, D.; Lohmann, U.; Raga, G.B.; O'Dowd, C.D.; Kulmala, M.; Fuzzi, S.; Reissell, A.; Andreae, M.O. Flood or drought: How do aerosols affect precipitation? *Science* **2008**, *321*, 1309–1313. [CrossRef]
32. Van Den Heever, S.C.; Cotton, W.R. Urban aerosol impacts on downwind convective storms. *J. Appl. Meteorol. Climatol.* **2007**, *46*, 828–850. [CrossRef]
33. Zhong, S.; Qian, Y.; Zhao, C.; Leung, R.; Yang, X.Q. A case study of urbanization impact on summer precipitation in the Greater Beijing Metropolitan Area: Urban heat island versus aerosol effects. *J. Geophys. Res. Atmos.* **2015**, *120*, 10903–10914. [CrossRef]
34. Chen, M.; Wang, Y.; Gao, F.; Xiao, X. Diurnal variations in convective storm activity over contiguous North China during the warm season based on radar mosaic climatology. *J. Geophys. Res.* **2012**, *117*, D20115. [CrossRef]
35. Li, H.; Cui, X.; Zhang, D.-L. On the initiation of an isolated heavy-rain-producing storm near the central urban area of Beijing metropolitan region. *Mon. Weather Rev.* **2017**, *145*, 181–197. [CrossRef]
36. Li, H.; Cui, X.; Zhang, D.L. A statistical analysis of hourly heavy rainfall events over the Beijing metropolitan region during the warm seasons of 2007–2014. *Int. J. Climatol.* **2017**, *37*, 4027–4042. [CrossRef]
37. Liu, L.; Ran, L.; Sun, X. Analysis of the structure and propagation of a simulated squall line on 14 June 2009. *Adv. Atmos. Sci.* **2015**, *32*, 1049. [CrossRef]
38. Yin, S.; Li, W.; Chen, D.; Jeong, J.; Guo, W. Diurnal variations of summer precipitation in the Beijing area and the possible effect of topography and urbanization. *Adv. Atmos. Sci.* **2011**, *28*, 725–734. [CrossRef]
39. Zhang, D.L.; Lin, Y.; Zhao, P.; Yu, X.; Wang, S.; Kang, H.; Ding, Y. The Beijing extreme rainfall of 21 July 2012:"Right results" but for wrong reasons. *Geophys. Res. Lett.* **2013**, *40*, 1426–1431. [CrossRef]
40. Ji, L.; Chen, H.; Li, L.; Chen, B.; Xiao, X.; Chen, M.; Zhang, G. Raindrop Size Distributions and Rain Characteristics Observed by a PARSIVEL Disdrometer in Beijing, Northern China. *Remote Sens.* **2019**, *11*, 1479. [CrossRef]
41. Ma, Y.; Ni, G.; Chandra, C.V.; Tian, F.; Chen, H. Statistical characteristics of raindrop size distribution during rainy seasons in the Beijing urban area and implications for radar rainfall estimation. *Hydrol. Earth Syst. Sci.* **2019**, *23*, 4153–4170. [CrossRef]
42. Jaffrain, J.; Studzinski, A.; Berne, A. A network of disdrometers to quantify the small-scale variability of the raindrop size distribution. *Water Resour. Res.* **2011**, *47*, W00H06. [CrossRef]
43. Tokay, A.; Wolff, D.B.; Petersen, W.A. Evaluation of the new version of the laser-optical disdrometer, OTT Parsivel2. *J. Atmos. Ocean. Technol.* **2014**, *31*, 1276–1288. [CrossRef]
44. Krajewski, W.F.; Kruger, A.; Caracciolo, C.; Golé, P.; Barthes, L.; Creutin, J.-D.; Delahaye, J.-Y.; Nikolopoulos, E.I.; Ogden, F.; Vinson, J.-P. DEVEX-disdrometer evaluation experiment: Basic results and implications for hydrologic studies. *Adv. Water Resour.* **2006**, *29*, 311–325. [CrossRef]
45. Jaffrain, J.; Berne, A. Experimental Quantification of the Sampling Uncertainty Associated with Measurements from PARSIVEL Disdrometers. *J. Hydrometeorol.* **2011**, *12*, 352–370. [CrossRef]
46. Tokay, A.; Petersen, W.A.; Gatlin, P.; Wingo, M. Comparison of raindrop size distribution measurements by collocated disdrometers. *J. Atmos. Ocean. Technol.* **2013**, *30*, 1672–1690. [CrossRef]
47. Brandes, E.A.; Zhang, G.; Vivekanandan, J. Experiments in Rainfall Estimation with a Polarimetric Radar in a Subtropical Environment. *J. Appl. Meteorol.* **2002**, *41*, 674–685. [CrossRef]
48. Beard, K.V.; Johnson, D.B.; Baumgardner, D. Aircraft observations of large raindrops in warm, shallow, convective clouds. *Geophys. Res. Lett.* **1986**, *13*, 991–994. [CrossRef]
49. Marzano, F.S.; Cimini, D.; Montopoli, M. Investigating precipitation microphysics using ground-based microwave remote sensors and disdrometer data. *Atmos. Res.* **2010**, *97*, 583–600. [CrossRef]
50. Testud, J.; Oury, S.; Black, R.A.; Amayenc, P.; Dou, X. The Concept of "Normalized" Distribution to Describe Raindrop Spectra: A Tool for Cloud Physics and Cloud Remote Sensing. *J. Appl. Meteorol.* **2001**, *40*, 1118–1140. [CrossRef]
51. Waterman, P. Matrix formulation of electromagnetic scattering. *Proc. IEEE* **1965**, *53*, 805–812. [CrossRef]
52. Bringi, V.N.; Chandrasekar, V. *Polarimetric Doppler Weather Radar: Principles and Applications*; Cambridge University Press: Cambridge, UK, 2001.
53. Liu, W.; You, H.; Ren, G.; Yang, P.; Zhang, B. Subtle Precipitation Characteristics in Beijing Area. *Clim. Environ. Res.* **2014**, *19*, 61–68. (In Chinese)

54. Yang, P.; Xiao, Z.; Shi, W. Fine-Scale Characteristics of Rainfall in Beijing Urban Area Based on a High-Density Autonomous Weather Stations (AWS) Dataset. *Chin. J. Atmos. Sci.* **2017**, *41*, 475–489. (In Chinese)
55. Zhang, D.-L. Rapid urbanization and more extreme rainfall events. *Sci. Bull.* **2020**, *65*, 516–518. [CrossRef]
56. Rosenfeld, D. Suppression of rain and snow by urban and industrial air pollution. *Science* **2000**, *287*, 1793–1796. [CrossRef]
57. Zhong, S.; Yang, X.-Q. Mechanism of urbanization impact on a summer cold-frontal rainfall process in the greater Beijing metropolitan area. *J. Appl. Meteorol. Climatol.* **2015**, *54*, 1234–1247. [CrossRef]
58. Ji, W.; Wang, Y.; Zhuang, D. Spatial distribution differences in PM2.5 concentration between heating and non-heating seasons in Beijing, China. *Environ. Pollut.* **2019**, *248*, 574–583. [CrossRef]
59. Ryzhkov, A.; Zrnić, D. Comparison of dual-polarization radar estimators of rain. *J. Atmos. Ocean. Technol.* **1995**, *12*, 249–256. [CrossRef]
60. Matrosov, S.Y. Evaluating polarimetric X-band radar rainfall estimators during HMT. *J. Atmos. Ocean. Technol.* **2010**, *27*, 122–134. [CrossRef]
61. Napoli, A.; Crespi, A.; Ragone, F.; Maugeri, M.; Pasquero, C. Variability of orographic enhancement of precipitation in the Alpine region. *Sci. Rep.* **2019**, *9*, 13352. [CrossRef]